# Hydrodynamic interactions of sheets vs filaments: Synchronization, attraction, and alignment

Sarah D. Olson and Lisa J. Fauci

Citation: Physics of Fluids **27**, 121901 (2015); doi: 10.1063/1.4936967
View online: http://dx.doi.org/10.1063/1.4936967
View Table of Contents: http://scitation.aip.org/content/aip/journal/pof2/27/12?ver=pdfcov
Published by the AIP Publishing

PHYSICS OF FLUIDS **27**, 121901 (2015)

# Hydrodynamic interactions of sheets vs filaments: Synchronization, attraction, and alignment

Sarah D. Olson[1,a)] and Lisa J. Fauci[2,b)]
[1]*Department of Mathematical Sciences, Worcester Polytechnic Institute, 100 Institute Road, Worcester, Massachusetts 01609, USA*
[2]*Department of Mathematics and Center for Computational Science, Tulane University, 6823 St. Charles Ave., New Orleans, Louisiana 70118, USA*

(Received 19 April 2015; accepted 3 November 2015; published online 23 December 2015)

The synchronization of nearby sperm flagella as they swim in a viscous fluid was observed nearly a century ago. In the early 1950s, in an effort to shed light on this intriguing phenomenon, Taylor initiated the mathematical analysis of the fluid dynamics of microorganism motility. Since then, models have investigated sperm hydrodynamics where the flagellum is treated as a waving sheet (2D) or as a slender waving filament (3D). Here, we study the interactions of two *finite* length, *flexible* filaments confined to a plane in a 3D fluid and compare these to the interactions of the analogous pair of *finite, flexible* sheets in a 2D fluid. Within our computational framework using regularized Stokeslets, this comparison is easily achieved by choosing either the 2D or 3D regularized kernel to compute fluid velocities induced by the actuated structures. We find, as expected, that two flagella swimming with a symmetric beatform will synchronize (phase-lock) on a fast time scale and attract towards each other on a longer time scale in both 2D and 3D. For a symmetric beatform, synchronization occurs faster in 2D than 3D for sufficiently stiff swimmers. In 3D, a greater enhancement in efficiency and swimming velocity is observed for attracted swimmers relative to the 2D case. We also demonstrate the tendency of two asymmetrically beating filaments in a 3D fluid to align — in tandem — exhibiting an efficiency boost for the duration of their sustained alignment. © *2015 AIP Publishing LLC*. [http://dx.doi.org/10.1063/1.4936967]

## I. INTRODUCTION

The classic work of Taylor in the early 1950s initiated the study of the hydrodynamics of microorganism motility by examining the progression of an infinite sheet undergoing small sinusoidal oscillations in a Stokesian fluid[1] and also an infinite cylindrical filament undergoing the same small oscillations.[2] Since then, there has been a wealth of experimental, computational, and analytical studies aimed at understanding hydrodynamic interactions of microorganisms. Taylor[1] showed that the in-phase configuration of two parallel sheets minimized the rate at which these idealized swimmers do work against the viscous fluid. Mettot and Lauga[3] recently extended Taylor's analysis[2] to show that infinite waving filaments in 3D dissipate the least amount of energy when they beat in-phase, consistent with the 2D sheets. The closer the sheets or filaments are to each other, the more energetically favorable the in-phase configuration is. Recent experiments by Woolley *et al*. demonstrate the dynamic phase-locking of swimming bull sperm.[4] Two nearby sperm flagella, initially beating with different phases and beat frequencies, interact through the viscous fluid to synchronize their beats and eventually attract, shown in panels (a)-(c) of Fig. 1. The swimmers also exhibited a marked increase in velocity (by several $\mu$m s$^{-1}$) when this synchronization and attraction occurred. The dynamics of flagellar synchronization and attraction occur as these elastic structures modulate their

a)sdolson@wpi.edu. URL: http://users.wpi.edu/~sdolson/. NSF DMS 1122461.
b)fauci@tulane.edu. URL: http://math.tulane.edu/~ljf/. NSF DMS 1043626.

 

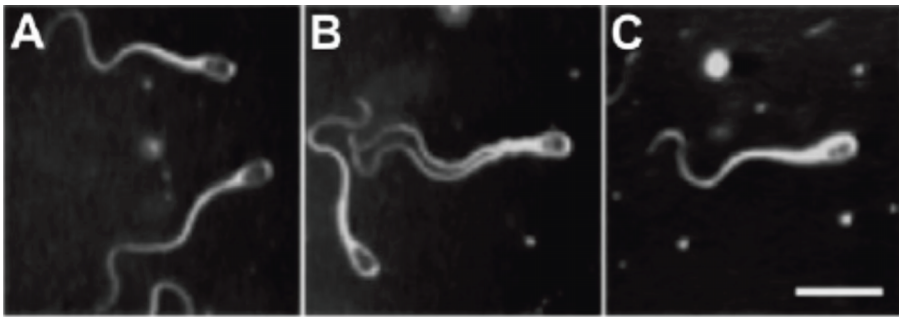


FIG. 1. Reproduced with permission from Woolley *et al.*, J. Exp. Biol. **212**, 2215–2223 (2009). Copyright 2009 Company of Biologists LTD. Panels (a)-(c) are three snapshots in time of bull sperm swimming in a fluid of viscosity similar to that of cervical mucus. (a) Initially, the two sperm are swimming with flagellar waveforms that are not in-phase. (b) Through hydrodynamic interactions, the two sperm synchronize and attract. (c) The two sperm exhibit full attraction and synchronization.

waveforms and as differences in their swimming velocities emerge due to interactions with the viscous fluid.

In the idealized model of parallel, identical, infinite sheets with prescribed phase-shifted waveforms of front-back symmetry, the time-reversibility of Stokes flow and symmetry arguments affirm that phase-locking cannot be achieved by swimming at different velocities.[5,6] Adding either flexibility to the sheets or viscoelasticity to the fluid does break this symmetry and phase-locking of these infinite sheets can occur.[7–9] Early computational studies demonstrated the dynamic synchronization of undulating, flexible sheets immersed in a 2D viscous, incompressible fluid at low but non-zero Reynolds number.[10]

When flagella are modeled by *finite* sheets in a 2D fluid, much of the restrictive symmetry imposed when considering infinite sheets is removed. In addition, unlike the case of infinite sheets which cannot attract due to the incompressibility of the fluid between them, finite sheets can indeed attract in a 2D fluid. Using an actuated Euler elastica model of flexible, finite flagella, Fauci and MacDonald[11] investigated synchronization of waveforms and demonstrated attraction of swimmers to each other in 2D. More recently, Yang *et al.*[12] used multiparticle collision dynamics in 2D to study both synchronization and attraction of actuated finite sheets. They observed a fast time scale of synchronization and a longer time scale of attraction.

How closely does a two-dimensional fluid model approximate the corresponding three-dimensional model — even in a very idealized system? When Taylor considered infinite sheets and filaments,[1,2] he showed that infinite filaments in a 3D fluid subjected to the same small amplitude kinematics as an infinite sheet governed by 2D fluid dynamics progressed more slowly than the sheet, with the ratio of corresponding speeds depending upon the thickness of the filament.[1,2] The ratio of swimming speeds is

$$\frac{V_{3D}}{V_{2D}} = \frac{K_0(\kappa a) - \frac{1}{2}}{K_0(\kappa a) + \frac{1}{2}}. \tag{1}$$

Here, $K_0$ is the 0-th order modified Bessel function of the second kind, $a$ is the filament radius, and $\kappa$ is the wavenumber of the flagellar oscillation. It is, of course, not surprising that differences arise when 2D fluid dynamics is used to approximate 3D dynamics.

Here, we investigate the hydrodynamic interactions of two coplanar filaments in a 3D fluid (Fig. 2(b)) and compare these to the interactions of the analogous pair of sheets in a 2D fluid (Fig. 2(a)). The swimmers considered here are finite and flexible. Moreover, while the *preferred kinematics* are prescribed, the realized kinematics emerge from the full coupling of the viscous fluid and the flexible structures. Flagellar forces due to a preferred planar waveform are derived from an energy functional, and these forces are coupled to either 2D or 3D Stokes flow. Within our computational framework using regularized Stokeslets, this is easily achieved by choosing either the 2D or 3D regularized kernel to solve for fluid velocities induced by the actuated structures. We examine the phase synchronization of nearby swimmers with symmetric beatforms, as well as the attraction of phase-locked swimmers

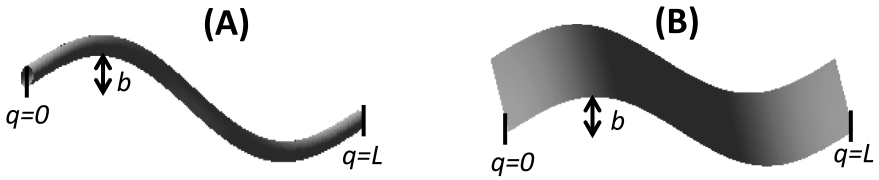


FIG. 2. Representation of Taylor's swimming sheet in (a) and 3D cylindrical filament in (b). The amplitude $b$ and arc length parameter $q$ are labeled on the structures.

towards each other. We find that synchronization for sufficiently stiff swimmers happens on a faster time scale for the 2D symmetric sheet, while efficiency increases and power decreases for both the symmetric sheets and filaments. In 3D, we observe increases in swimming speed and efficiency for attracted filaments. We also examine the interaction of two swimmers whose preferred waveforms, like hyperactivated mammalian sperm, are asymmetric.[13,14] A single asymmetric swimmer, whose planar bends are more pronounced on one side, would trace out a circular trajectory in free space. Here, we report the tendency for two asymmetric swimming filaments in a 3D fluid to transiently align, in tandem. This "sperm train" results in an efficiency boost for the duration of the filaments' alignment.

## II. MATHEMATICAL MODEL

In order to compare the dynamics of 2D sheets to those of filaments interacting in 3D, we only consider filaments whose centerlines are confined to the same plane. In an unbounded fluid, symmetry arguments affirm that the motion of these filaments will remain in that plane. In both 2D and 3D, each of the two flagellar centerlines is modeled as a generalized Euler elastica whose shape changes are driven by the pursuit of a preferred curvature wave.[15–17] The force per unit length $\mathbf{g}_i$ supported by the $i$th flageller centerline $\mathbf{X}_i(q,t)$ is derived from tensile and bending energies,

$$\varepsilon_{i,tens} = S_T \int_0^L \left( \left\| \frac{\partial \mathbf{X}_i}{\partial q} \right\| - 1 \right)^2 dq \,, \tag{2a}$$

$$\varepsilon_{i,bend} = S_B \int_0^L \left( \frac{\partial \Theta_i}{\partial q} - \zeta_i(q,t) \right)^2 dq \,. \tag{2b}$$

Here, $q$ is an arclength parameter, $0 \le q \le L$, $\Theta_i$ is the shear angle, and $\zeta_i(q,t)$ is the time-dependent *preferred curvature* that drives the swimming motion of the flagellum. The stiffness coefficients $S_T$ and $S_B$ control how strictly the emergent waveform conforms with the preferred waveform. For simplicity, these stiffness constants are chosen to be the same for both flagella. By choosing the stiffness coefficient $S_T$ sufficiently large, the flagella are effectively inextensible since Eq. (2a) limits stretching and compression. The bending energy $\varepsilon_{i,bend}$ in Eq. (2b) is minimized if the actual curvature $\partial\Theta_i/\partial q$ is equal to the preferred curvature $\zeta_i$. Below we will discuss how we choose preferred curvature to simulate observed sperm motility patterns.

The force per unit length $\mathbf{g}_i$ concentrated at each material point of the flagellar centerline is defined by

$$\mathbf{g}_i \, dq = -\frac{\partial(\varepsilon_{i,tens} + \varepsilon_{i,bend})}{\partial \mathbf{X}_i}. \tag{3}$$

These forces are coupled to an unbounded viscous fluid by the incompressible Stokes equations,

$$0 = -\nabla p + \mu \Delta \mathbf{u} + \sum_{i=1}^{2} \int_0^L \mathbf{g}_i(\mathbf{X}_i(q,t),t) \phi_\delta(\mathbf{x} - \mathbf{X}_i(q,t)) dq, \tag{4a}$$

$$0 = \nabla \cdot \mathbf{u}. \tag{4b}$$

Here, $\mathbf{u}$ is the fluid velocity, $\mathbf{x}$ is any point in free space (2D or 3D) $\mu$ is the dynamic viscosity, $p$ is the pressure, and $\mathbf{X}_i(q,t)$ is the $i$th flagellar centerline. The force per unit length that each flagellum exerts on the fluid $\mathbf{g}_i$ is supported along its centerline, but regularized by a 2D or 3D blob function $\phi_\delta$.

The regularization distributes forces supported on the centerline to a small volume of fluid around the curve. While one may regard the blob function $\phi_\delta$ as a regularized Dirac delta function, we treat the regularization parameter $\delta$ as a physical parameter chosen to be on the order of the flagellar radius.[17,18] Here, we choose the blob functions

$$\phi_\delta(r) = \frac{3\delta^3}{2\pi(r^2+\delta^2)^{5/2}} \quad \text{(2D)}, \tag{5a}$$

$$\phi_\delta(r) = \frac{15\delta^4}{8\pi(r^2+\delta^2)^{7/2}} \quad \text{(3D)}, \tag{5b}$$

where $r = \|\mathbf{x}\|$.

For a single point force $\mathbf{g}_k$ concentrated at a point $\mathbf{X}_k$, these choices of $\phi_\delta$ give rise to the regularized Stokeslets,

$$\mathbf{u}_{2D}(\mathbf{x}) = \frac{-\mathbf{g}_k}{4\pi\mu}\left(\ln(R_k+\delta) - \frac{\delta(R_k+2\delta)}{(R_k+\delta)R_k}\right) + \frac{1}{4\pi\mu}\left(\frac{[\mathbf{g}_k\cdot(\mathbf{x}-\mathbf{X}_k)]\,(\mathbf{x}-\mathbf{X}_k)(R_k+2\delta)}{(R_k+\delta)^2R_k}\right), \tag{6a}$$

$$\mathbf{u}_{3D}(\mathbf{x}) = \frac{1}{8\pi\mu}\left(\frac{r_k^2+2\delta^2}{R_k^3}\mathbf{g}_k + \frac{[\mathbf{g}_k\cdot(\mathbf{x}-\mathbf{X}_k)]\,(\mathbf{x}-\mathbf{X}_k)}{R_k^3}\right), \tag{6b}$$

where $r_k = \|\mathbf{x}-\mathbf{X}_k\|$ and $R_k = \sqrt{r_k^2+\delta^2}$. These regularized Stokeslets are exact solutions of the Stokes equations and are everywhere incompressible.[19,20] Because the Stokes equations are linear, we may determine the fluid velocity due to a collection of concentrated forces by summing up the regularized Stokeslets centered at the points where forces are applied. These fluid velocities are defined everywhere, even at points on the centerlines of the flagella where forces are exerted. We evolve the coupled fluid-elastica system by requiring that the material points of the flagellar centerline move at the local fluid velocity

$$\frac{d\mathbf{X}_i}{dt}(q,t) = \mathbf{u}(\mathbf{X}_i(q,t),t), \quad i = 1,2. \tag{7}$$

### A. Preferred curvature

Propagating curvature waves have been observed in human sperm flagella using high speed imaging.[21] Symmetric bending, called activated motility, is often seen in mammalian sperm when the cytosolic calcium concentration is at a basal or resting level. Such symmetric bends passed along an isolated sperm flagellum will result in linear swimming trajectories.[22,23] Highly asymmetric planar waves, with flagellar amplitude much more pronounced in one direction, correspond to higher cytosolic calcium concentrations. This hyperactivated motility leads to circular swimming trajectories.[13,14,23,24]

The swimming motion of a flagellum is due to the action of dynein molecular motors that use energy from ATP dephosphorylation to generate sliding between adjacent microtubule doublets that comprise the axoneme.[25] The presence of other passive elastic structural forces converts this sliding to bending.[26,27] While previous computational studies have examined the action of individual model dyneins on elastic filaments to produce flagellar waveforms,[28] here we take a simplified approach that does not attempt to capture the details of internal force generation, but instead assumes that the elastic flagellum is in pursuit of a preferred wave of curvature. We assume this preferred wave is sinusoidal for symmetric swimmers and asymmetric for hyperactivated swimmers, based on previous experimental studies.[13,21] We guide the sheet or filament centerlines to pursue planar sinusoidal waves of the form $\mathbf{X}_i(q,t) = (q, b(q,t)\sin(\kappa q - \omega t - \psi_i), 0)$, where $b(q,t)$ is amplitude, $\omega$ is frequency, and $\psi_i$ is a phase shift. Such preferred kinematics corresponds to the preferred curvature

$$\zeta_i(q,t) = -b(q,t)\kappa^2\sin(\kappa q - \omega t - \psi_i) \tag{8}$$

that we note has been used in previous models.[11,16,17,29] We choose

$$b(q,t) = \begin{cases} b_{A,1} & \text{for } \sin(\kappa q - \omega t - \psi_i) < 0, \\ b_{A,2} & \text{for } \sin(\kappa q - \omega t - \psi_i) > 0. \end{cases} \tag{9}$$

TABLE I. Parameters for swimmers in 3D (finite filament) and 2D (finite sheet).

| | |
|---|---|
| $L$, filament length | 1 |
| $M$, points on swimmer | 101 |
| $\delta$, regularization parameter | 0.01 |
| $S_T$, tensile stiffness | 100 (3D), 10 000 (2D) |
| $S_B$, bending stiffness | 0.025 (3D), 2.5 (2D) |
| $\Delta t$, time step | $5 \times 10^{-7}$ |
| $\kappa$, wavenumber | $2\pi/L$ |
| $b$ (symmetric case), amplitude | 0.1 |
| $b_{A,1}$, $b_{A,2}$ (asymmetric case) | 0.075, 0.1125 |
| $\omega$, frequency | $2\pi$ |

In the case where $b_{A,1} = b_{A,2}$, our preferred flagellar beat would be symmetric. Asymmetric (hyperactivated) flagellar beats are achieved by choosing $b_{A,1} \neq b_{A,2}$.

## III. RESULTS

We nondimensionalize the Stokes equations and tensile and bending energies using a viscosity of water and length and time scales representative of a mouse sperm, as detailed previously in the work of Olson *et al.*[17] The nondimensional flagellar length of $L = 1$ corresponds to 100 $\mu$m (mouse sperm is 120 $\mu$m[30]), and a nondimensional beat period of $T = 1$ corresponds to a flagellar beat frequency of 10 Hz. Previous experiments have recorded amplitudes of flagellar bending in the range of 2-20 $\mu$m.[21,23] The nondimensional amplitude $b = 0.1$ corresponds to 10 $\mu$m. For filaments in a 3D fluid, the flexural rigidity of the elastic flagellar centerline achieved by choosing $S_T = 25$–$125$ and $S_B = 0.025$–$0.075$ is on the order of $5 \times 10^{-21}$ Nm$^2$, which falls in the range of bull sperm ($4$–$27 \times 10^{-21}$ Nm$^2$)[31] and rat sperm ($1$–$10 \times 10^{-19}$ Nm$^2$).[32] The corresponding stiffnesses for a sheet in a 2D fluid are calibrated so that the achieved kinematics of the flagellar centerline in a baseline case of a symmetric swimmer are approximately the same as those of the centerline for the corresponding filament in 3D. We note that model parameters, summarized in Table I, have been shown to result in flagellar swimming velocities characteristic of human and mouse sperm for both symmetric and asymmetric swimmers.[17] To represent other species, we use a range of bending modulus $S_B$ in simulations where an increased (decreased) stiffness generally corresponds to a small increase (decrease) of 0.02–0.05 in achieved average amplitude. In the numerical simulations presented here, the flagellar centerlines are discretized into $M = 101$ points and Eq. (7) is solved using the forward Euler method with time step $\Delta t = 5 \times 10^{-7}$.

Fig. 3 shows the achieved flagellar waveforms for the sheet in 2D (panel (a)) and the filament in 3D (panel (b)) during a single period of flagellar oscillation. The first material points of the flagellar centerlines are superimposed in each panel for the different time points. We emphasize that the kinematics of the flagellar centerline are not prescribed. Even for a single swimmer in an unbounded fluid, the emergent waveform will differ from the preferred waveform due to the viscous coupling. While the preferred nondimensional amplitude $b = 0.1$ was input for both the sheet and the filament in Fig. 3,

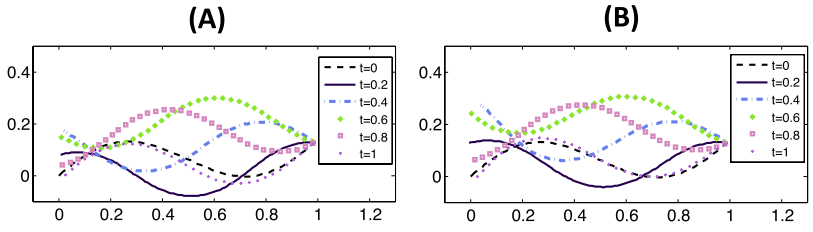


FIG. 3. Flagellar envelopes for (a) a finite sheet in a 2D fluid and (b) a finite filament in a 3D fluid. A wave is propagated to the left. Six snapshots of the flagellum within one beat period are superimposed such that the material point on the right is fixed.

the averaged achieved amplitude for both was $b_a = 0.108$. Small differences between the swimmers can be seen in Fig. 3, such as the larger deflection in the tail for the filament in a 3D fluid at $t = 0.4$ and $t = 0.6$. The swimming velocity of the finite sheet in 2D, averaged over a beat period, was computed to be $V_{2D} = 0.39$, and the corresponding averaged filament velocity $V_{3D} = 0.29$. The computed ratio of velocities for these finite, flexible swimmers is $V_{3D}/V_{2D} = 0.74$. Choosing the flagellar radius $a$ to be the blob parameter $\delta$, the ratio given by Eq. (1) for the corresponding infinite sheets and filaments in Taylor's asymptotics is[1,2] $V_{3D}/V_{2D} = 0.70$.

### A. Phase locking

Here, we examine the synchronization of flagellar centerlines whose preferred kinematics share identical amplitudes, wavelengths, and frequencies, but differ by a phase shift. Their flexural rigidities are also identical. In Fig. 4, a time progression of flagellar waveforms is shown for the sheets in panels (a)-(d) and for the filaments in panels (e)-(h). In both 2D and 3D, the two swimmers are initialized in a vertical distance of $d = 0.25$ apart with a phase shift of $\psi = \pi/2$ (panels (a) and (e)). As the wave propagates to the left, the swimmers progress to the right. A heuristic measure of synchrony is the alignment of the crests of the waves as the flexible flagella modulate their swimming velocities and shapes.

As in previous studies of the synchronization of flexible, infinite sheets,[8,9] the realized shapes of these interacting finite swimmers differ dramatically from the sinusoids they are in pursuit of (e.g., the top swimmer in panels 4(b) and 4(f)). In Fig. 4, we chose time points at which the shapes achieved by the sheets and filaments were similar. In both cases, the temporal beat periods of all flagellar waves are $T = 1$. In panels 4(d) and 4(h), we see that the crests of the pair of 2D and 3D swimmers have mostly aligned at $t = 0.0625$ and $t = 0.18$, respectively. While this synchronization occurs very early during the beat cycle in both cases, the sheet synchrony occurs much more quickly than the filament synchrony. We note that phase locking is observed in this model with out of phase forcing since the achieved shape of the flagellum emerges due to the fluid-structure interaction.

In order to further characterize synchronization, we examine the swimming speeds and power expended for each individual sheet and filament during the first half of the first beat (Fig. 5). For swimmers with identical actuation and material properties, a perfectly synchronized state would yield identical swimming velocities and power expenditures for each swimmer. In Fig. 5(a), we see that for both the 2D sheets and 3D filaments, the top swimmer initially exhibits greater swimming speed, with the difference much more pronounced in the 2D case. This relative difference in velocities along with the shape changes of the flexible swimmers allows them to evolve into a synchronized state. Fig. 5(a) indicates that the 2D swimmers have approximately the same swimming speed near time $t = 0.2$, while for the 3D swimmers, this occurs at about $t = 0.3$.

We define the power $P_i(t)$ of the $i$th flagellar centerline as

$$P_i(t) = \int_0^L [\mathbf{g}_i(\mathbf{X}_i(q,t),t) \cdot \mathbf{u}(\mathbf{X}_i(q,t),t)]\, dq, \tag{10}$$

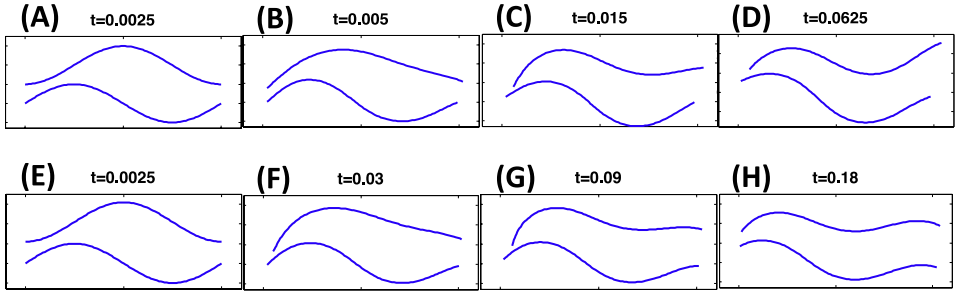


FIG. 4. Waveforms for two sperm initialized with a phase shift of $\psi = \pi/2$ and stacked a distance of $d = 0.25$ apart. Panels (a)-(d) correspond to the sheet in a 2D fluid and panels (e)-(h) correspond to a filament in a 3D fluid. Note that the times of the snapshots chosen are different in 2D and 3D — phase synchronization occurs on a faster time scale in 2D.

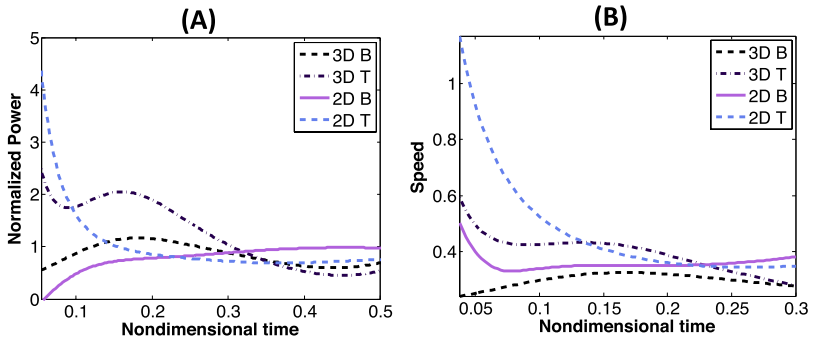


FIG. 5. Evolution of swimming speed (panel (a)) and normalized power expenditure (panel (b)) for the pairs of sheets and filaments with identical preferred shapes, but with an initial phase shift of $\psi = \pi/2$. In the insets of the figure, T and B correspond to the top and bottom swimmers in Fig. 4, respectively.

where integration is over the sheet or filament centerline, $\mathbf{g}_i$ is the force, and $\mathbf{u}(\mathbf{X}_i(q,t),t)$ is the velocity defined on the swimmer. Because the forces scale differently in 2D and 3D, in order to compare the evolution of power expenditures of the pairs of sheets or filaments as they synchronize, we normalize $P_i(t)$ by the average power of the corresponding *isolated* single sheet or filament in the respective fluid domain. Fig. 5(b) shows the time evolution of the normalized power for each individual sheet or filament. A similar trend to that of velocity is seen; the top swimmers have increased power initially and within a short period of time, before quickly equalizing.

To further investigate synchronization of sheets and filaments, we show results for several cases of bending stiffness $S_B$ and phase difference $\psi$. The phase locking time is calculated in terms of the number of nondimensional beats at which the speed and power difference between the two swimmers is less than 0.005 for at least one-tenth of a beat period. In Figs. 6(a)-6(c), for sufficiently stiff swimmers ($0.5\text{-}1 \times S_B$), we observe that phase locking occurs on a faster time scale for the 2D sheets than for the 3D filaments. For the 2D sheets initialized 0.5 and 0.75 apart, the synchronization time decreases as stiffness increases. When the vertical separation is smaller in 6(a), we observe that larger phase shifts correspond to larger times to phase locking for the 2D sheets. The 3D filaments exhibit a non-monotonic relationship (parabolic) between the stiffness and the time to phase lock for all three separation distances shown in Figs. 6(a)-6(c). The floppiest 3D filaments are able to interact and modify their waveforms quickly in order to phase lock the fastest for all three initialized separation distances.

## B. Transverse dynamics for filament pairs

The interpretation of a two-dimensional fluid model is that there is no change in state variables when moving out of that plane. However, in 3D, this is not true, even for a filament undergoing planar undulations. As in recent work by Mettot and Lauga[3] for infinite filaments, we show computed instantaneous flow fields and pressure fields in a plane transverse to a pair of identical finite filaments

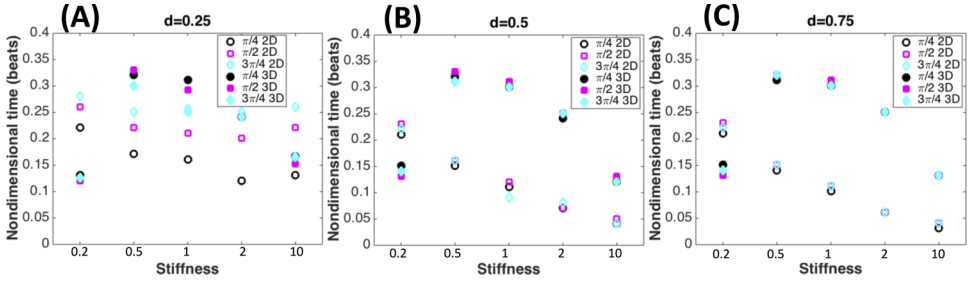


FIG. 6. Phase locking time for different bending rigidities $0.2S_B$, $0.5S_B$, $S_B$, $2S_B$, and $10S_B$. Three phase differences for the 2D sheet and 3D filament are shown ($\psi = \pi/4, \pi/2, 3\pi/4$). (a) Initial distance apart is $d = 0.25$, (b) $d = 0.5$, (c) $d = 0.75$.

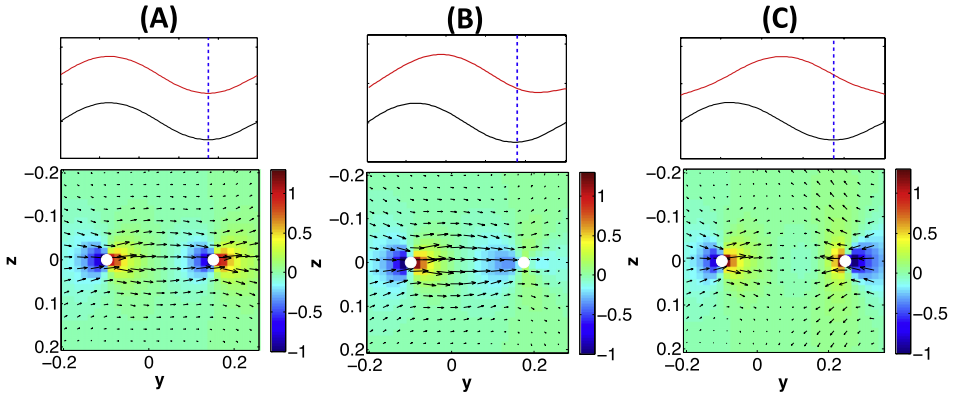


FIG. 7. The finite filament centerlines in a 3D fluid are shown in the top row. The bottom row shows the flow fields (arrows) and pressure contours (colorbar) projected onto the transverse plane $x = 0.75$ for two flagella at $t = 0.001\,25$. Column (a): $\psi = 0$ (in phase). Column (b): $\psi = \pi/4$. Column (c): $\pi/2$. The flagella cross sections are depicted in the bottom panel as white circles.

initialized at different phases. The filaments are in the $x$–$y$ plane ($z = 0$), and their cross sections are shown with white circles in the $y$–$z$ plane at $x = 0.75$. For the in-phase swimmers, Fig. 7(a), the flow is in the positive $y$ direction corresponding to the lower peak of the sine wave pushing up. There is minimal flow in the $z$ direction. The flow is much smaller in the positive $y$ direction for the upper filament in Fig. 7(b) when $\psi = \pi/4$. When the filaments are $\psi = \pi/2$ out of phase initially, a flow in the negative $y$ direction is created by the top filament as shown in Fig. 7(c).

### C. Attraction

We next examine attraction of two finite, flexible flagellar centerlines whose preferred kinematics share the identical amplitudes, wavelengths, and frequencies shown in Table I. Tensile and bending stiffness coefficients are also shown in Table I. Because attraction occurs on a much longer time scale than synchronization due to translational resistance,[12,33] we initialize two swimmers that are already in phase ($\psi = 0$) at a distance of $d = 0.25$ apart. The preferred flagellar waveforms are symmetric with constant amplitude for both of the 2D sheets and the 3D filaments. Figs. 8(a) and 8(b) show the

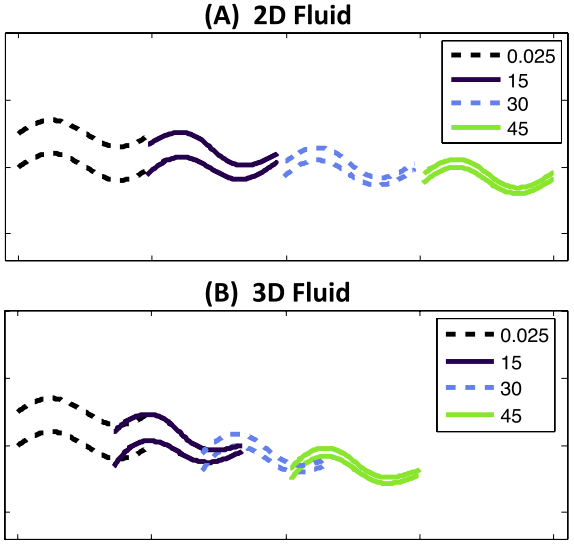


FIG. 8. Snapshots of flagellar centerlines for two sperm initialized in phase ($\psi = 0$) and stacked a distance of $d = 0.25$ apart, with preferred kinematic parameters from Table I. In (a), sheets in a 2D fluid and in (b), filaments in a 3D fluid. In both (a) and (b), the waveforms are shown at $t = 0.025$, $t = 15$, $t = 30$, and $t = 45$.

swimming progression of the 2D and 3D swimmers, respectively, up through forty-five beat periods. We note that the attraction does not progress uniformly along the flagellar centerlines, with the gap between the head points closing more dramatically than that between the tail points at $t = 15$, for instance.

We found that the dynamics of attraction depend upon the initial distance between the two swimmers and the flagellar bending rigidity. This bending rigidity is determined by the choice of the stiffness coefficient $S_B$ that controls how closely the bending energy in Eq. (2b) is minimized. We note that different species of sperm can have a flexural rigidity varying by two to three orders of magnitude. In Fig. 9, we measure the evolution of attraction of three pairs of swimmers with different bending rigidities $((1/5)S_B, S_B, 5S_B)$ in both 2D and 3D. The first column shows the distance between the head points as a function of time, and the second column shows the distance between the tail points. Each pair of swimmers was initialized at a distance of $d = 0.25$, 0.5, or 0.75 apart at $t = 0$. We note that when the distance between two points on the sheets or filaments is less than $4\delta = 0.04$ (twice the flagellar diameter), we turn on a repulsive force to ensure that the structures do not self cross. The repulsive force acts like one due to a compressed Hookean spring, whose stiffness coefficient $S_R$ is chosen to ensure that this repulsive force is at least an order of magnitude smaller than the bending and tensile forces. The repulsive force is not on continually; it is only nonzero at time steps where points on the structure are less than $4\delta = 0.04$ apart.

Fig. 9(a) demonstrates that the stiffer sheets ($S_B$ and $5S_B$) are able to attract and reach a steady state distance of 0.046-0.05 apart at the head ($4\delta$ is the minimum allowed based on the repulsion term). We observe a nontrivial "saturation" where an increase in stiffness of $S_B$–$5S_B$ has very similar dynamics of attraction. However, the floppier 2D sheets with bending stiffness $(1/5)S_B$ are not able to fully attract and level off at a distance of 0.055 apart. In this graph, for the initial distances used, we observe a similar time scale of attraction in 2D for all three cases of bending stiffness. Fig. 9(c) shows the evolution of the distances between the head points of the corresponding 3D filaments. As in the 2D case, the stiffer swimmers are able to reach the minimum distance between the heads or fronts of the swimmer. Note that the attraction of head points occurs more quickly for filaments than

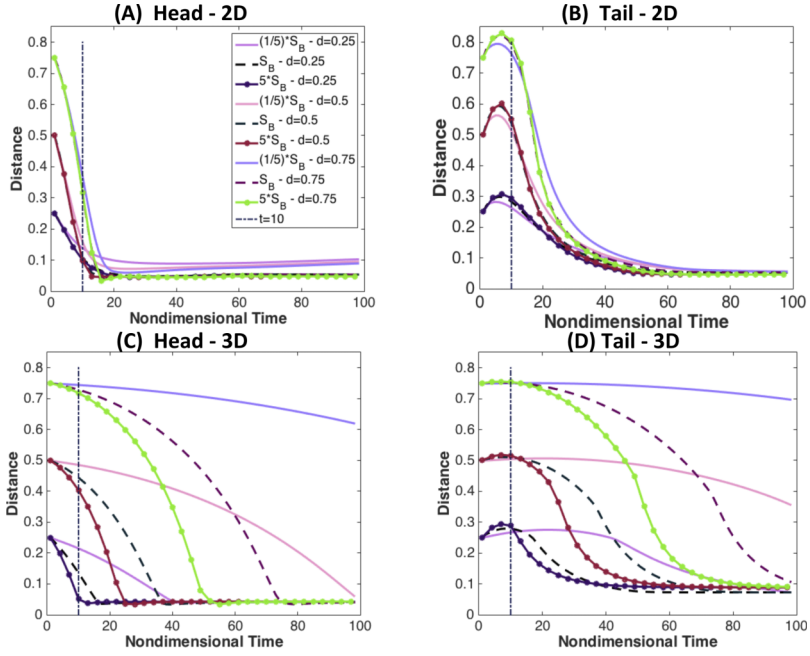


FIG. 9. Evolution of distances between the head points (a) for sheets and (c) for filaments as they attract with different bending rigidities and different starting locations. The sperm are initially stacked at a vertical distance of $d = 0.25$, 0.5, or 0.75 apart. Corresponding distance between tail points for sheets in (b) and filaments in (d). The legend indicating stiffness and initial distances is given in (a) and is the same for (b)-(d). ($S_B$ corresponding to the baseline value given in Table I.)

sheets for the case $d = 0.25$, with full attraction after approximately 10 ($5S_B$) and 15 ($5S_B$) beats. In contrast to the 2D case in Fig. 9(a), the time scale of attraction for the 3D filaments increases as the distance between the swimmers increases. Additionally, the time scale of attraction increases as bending stiffness decreases. For all cases, the 3D head distance eventually sustains a distance apart that is around 0.041, close to the minimum distance of 0.04 allowed. Thus, once the 3D swimmers have attracted, they are able to have a smaller distance between the head points than the 2D swimmers for all cases. In contrast, the gaps between the tail points (Figs. 9(b) and 9(d)) do not close as quickly as those between the head points. Additionally, the distance between the tail points actually increases initially, as the heads turn towards each other. For the 2D tail distance in Fig. 9(b), we observe similar dynamics as the head distance in Fig. 9(a), times for attraction remain constant at the tail for different starting distances. We note that the stable long term distance between the tail points of the 2D swimmers is the same as the head distance for all cases. For the distance $d = 0.25$, the stiffer 3D swimmers in Fig. 9(d) are able to reach a minimal tail distance faster than the corresponding 2D swimmers in Fig. 9(b). Similar to the 3D head distance in Fig. 9(c), the decrease of the distance between the tail points in 3D shown in Fig. 9(d) depends on the bending stiffness and initial distance apart. We note that the tail distance does decrease to a minimal value around 0.07-0.08 for the stiffer swimmers. For the case of the floppiest swimmer ($(1/5)S_B$) starting $d = 0.75$ apart, it takes more than 100 beat periods to reach the minimal distance apart.

Do attracting sheets and filaments swim faster than a single isolated swimmer with the same preferred kinematics? Does the swimming become more efficient as they attract? Fig. 10 reports the velocity of attracting sheets (panel (a)) and filaments (panel (c)) initialized $d = 0.25$ apart, normalized by the velocity of the corresponding solo swimmer. The velocity we report here is the velocity of the center of mass of the swimmer, time averaged over each period of flagellar beating. Since the top and bottom swimmers exhibit almost identical velocities and efficiencies, we only show the curve for the top swimmer in each case. In each individual simulation, we see that swimming speed increases initially as the swimmers attract. Compared to a single swimmer, however, Fig. 10(a) shows that

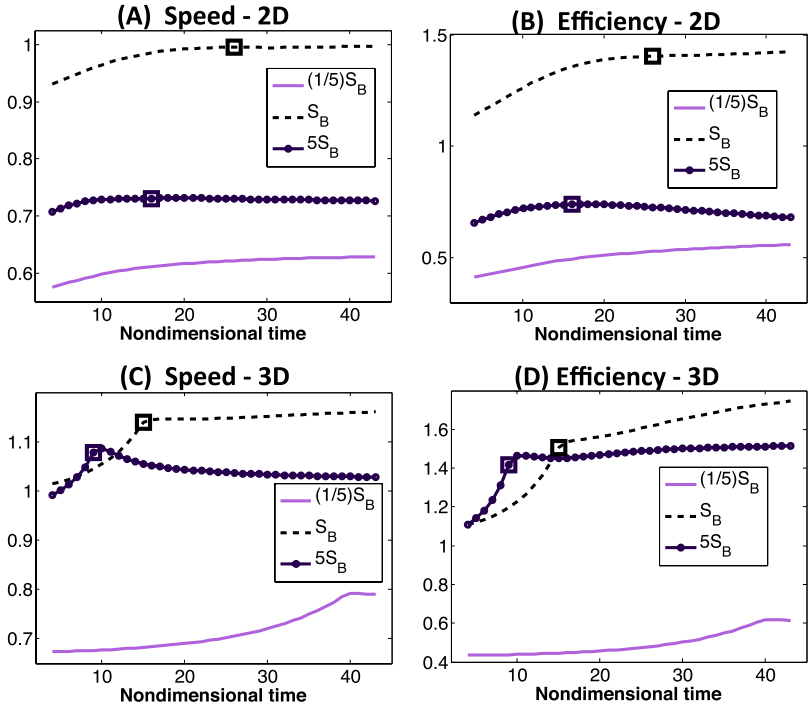


FIG. 10. Swimming speeds of attracting swimmers initialized $d = 0.25$ apart and normalized by that of the corresponding solo swimmer: (a) sheets and (c) filaments. Efficiencies of attracting swimmers normalized by that of the corresponding solo swimmer: (b) sheets and (d) filaments. The squares denote for the first time that the repulsion time is nonzero at any point along the swimmer.

attracting sheets always swim more slowly than the corresponding single swimmer, with only the stiffest swimmers approaching the speed of the single swimmer as they attract. In contrast, Fig. 10(c) shows that the stiffest attracting filaments are able to achieve swimming speeds greater than that for a single filament. An enhancement in swimming speed for attracted and synchronized sperm has also been observed in the experiments.[4] The time that repulsion turns on is denoted with a square on each of the curves; additional enhancement in swimming speed beyond this time is not seen.

We define efficiency $\mathrm{Eff}_i$ of the $i$th swimmer as follows:

$$\mathrm{Eff}_i = \frac{(V_i)^2}{\langle P_i \rangle}, \tag{11}$$

where power $\langle P_i \rangle$ is the average power defined in Eq. (10) over one flagellar beat and $V_i$ is the time averaged velocity shown in Figs. 10(a) and 10(c). The efficiency of the attracted swimmers, normalized by the efficiency of the corresponding solo swimmer, is shown in Figs. 10(b) and 10(d). In each individual simulation, the sheets and filaments initially show an increase in normalized efficiency as they attract. Moreover, Figs. 10(b) and 10(d) show that attracted swimmers with bending stiffness $S_B$ achieve efficiencies more than 1.4 times that of the corresponding single swimmer. This enhancement in efficiency for the filament in 3D is much greater than that in the 2D fluid. The stiffest ($5S_B$) attracted filaments in 3D also exhibit greater efficiencies than a solo filament, but the stiffest sheets do not. For the floppiest sheets and filaments ($(1/5)S_B$), the efficiencies compared to the single swimmer are significantly less. We note that once the swimmers have attracted, we observe similar enhancements in swimming speed and efficiency for swimmers initialized with a vertical separation of $d = 0.5$ and 0.75 for both the 2D sheets and 3D filaments.

### D. Asymmetric swimmers

Hyperactivated motility in mammalian sperm occurs when there is an increased calcium concentration within the flagellum.[13,14,23,24] Hyperactivation is characterized by high amplitude, asymmetric waveforms that are thought to facilitate detachment from oviductal epithelia as well as penetration of the oocyte cumulus complex. As described in Eq. (9), an asymmetric shape can be achieved in the model flagellum by setting the preferred amplitude of bending in one direction different from the other. Unlike the symmetric swimmers considered in Secs. III A–III C, an isolated swimmer pursuing such asymmetric beat kinematics would traverse a circular path rather than a straight line. In Fig. 11(a), a trajectory for the asymmetric swimming sheet with parameters from Table I is shown, and the trajectory of the corresponding swimming filament is shown in Fig. 11(b). Here, the head point is tracked once per beat period, with the starting location denoted with a diamond. We see that each swimmer traverses a counter clockwise trajectory for the given asymmetry in amplitude, with

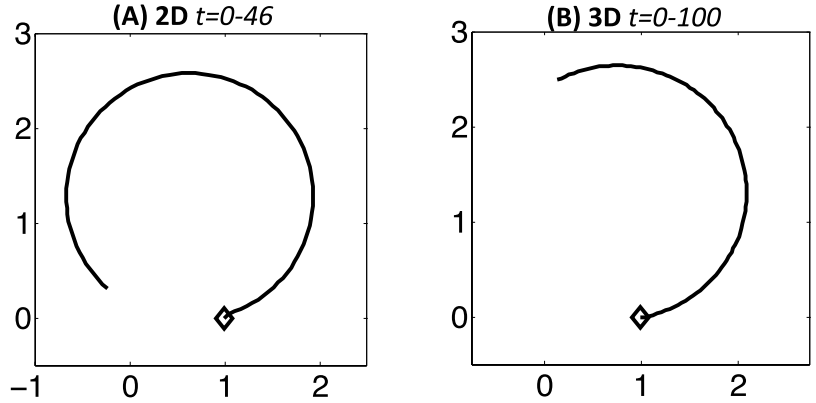


FIG. 11. Trajectories for a single asymmetric swimmer: (a) 2D fluid and (b) 3D fluid. The head point is plotted once per beat period and the diamond denotes the starting point. The curvature of the sheet's circular trajectory is $c_{2D} = 0.77$, and the curvature of the filament's circular trajectory is $c_{3D} = 0.75$.

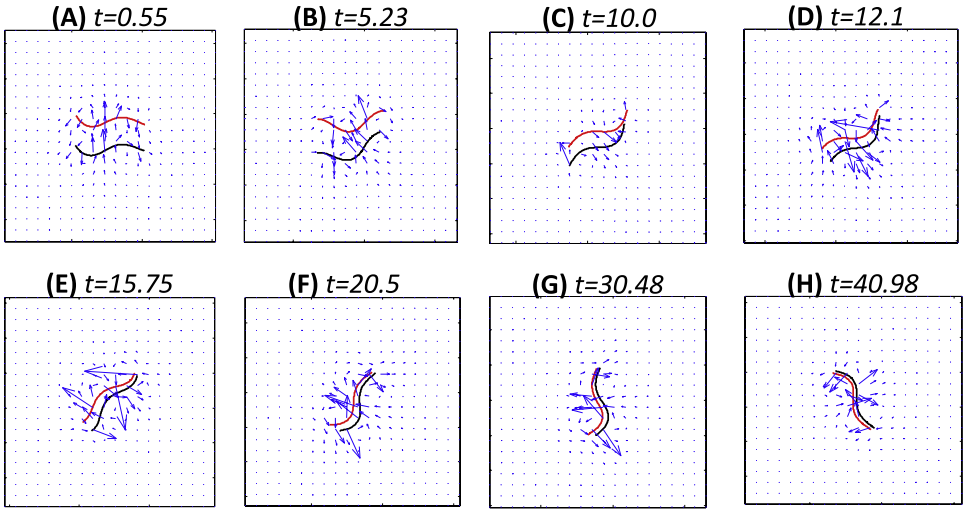


FIG. 12. The 2D flow field is shown at various time points for the asymmetric sheets. In this simulation, the sperm are initialized $d = 0.4$ apart. The corresponding trajectories are shown in Fig. 14(a).

the 2D sheet progressing further around the circle than the filament. We now examine the interaction of pairs of such flagella and investigate how their asymmetry affects the dynamics of attraction and their achieved trajectories. The full fluid-structure interaction will be studied for forty to one-hundred beat periods to give a sense of the long term behavior.

We first consider a pair of sheets in pursuit of the same asymmetric waveform, initialized in phase ($\psi = 0$) at a distance of $d = 0.4$ apart. The flow field and corresponding flagellar waveforms are shown at several time points in Fig. 12 (2D fluid). The corresponding pair of asymmetric filaments are shown in Fig. 13 (3D fluid). In both the 2D and 3D cases, Figs. 12(a)-12(d) and 13(a)-13(d) demonstrate flagellar attraction, even as the swimming direction rotates. After the swimmers have attracted, they remain attracted (Figs. 12(e)-12(h) and 13(e)-13(h)). The trajectories of each pair of swimmers are shown in Figs. 14(a) and 14(c) for the sheets and the filaments, respectively. Again, this corresponds to tracking the head point one time per beat period, with the starting points denoted with diamonds. The rectangles on the trajectories denote positions of the head points at the first instant

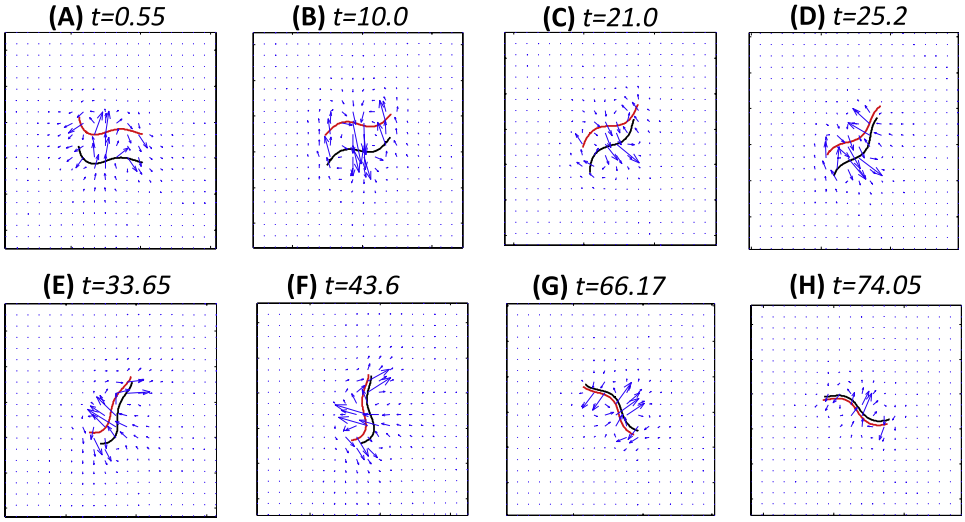


FIG. 13. The projected 3D flow field in the plane of the swimmers is shown at various time points for the asymmetric filaments. In this simulation, the sperm are initialized $d = 0.4$ apart. The corresponding trajectories are shown in Fig. 14(c).

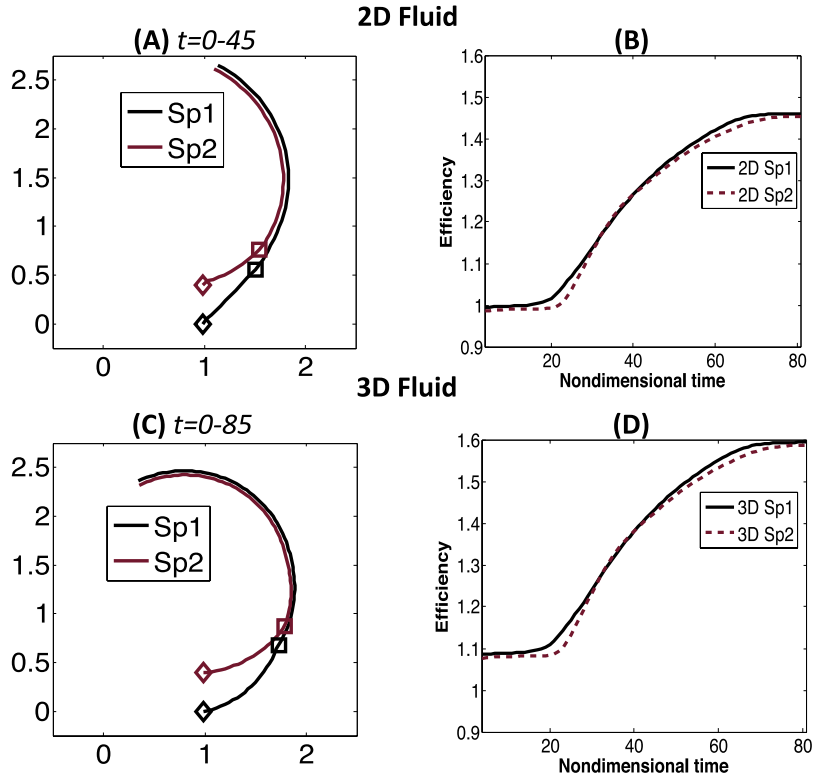


FIG. 14. (a) Trajectories of head points of sheets in a 2D fluid corresponding to Fig. 12. (b) Temporal evolution of the efficiencies of the sheets normalized by the efficiency of the corresponding solo swimmer. (c) Trajectories of head points of filaments in a 3D fluid corresponding to Fig. 13. (d) Temporal evolution of the efficiencies of the filaments normalized by the efficiency of the corresponding solo swimmer. Diamonds denote starting points, and rectangles denote the time at which repulsion is first turned on.

where a repulsion force was non-zero. While the curvature of the trajectory of the attracted swimming sheets ($c_{2D} = 0.74$) is largely unchanged from that of the corresponding isolated sheet trajectory ($c_{2D} = 0.77$), the curvature of the trajectory of the attracted swimming filaments ($c_{3D} = 0.97$) is significantly larger than that of the corresponding isolated filament ($c_{3D} = 0.75$).

The temporal evolution of the normalized efficiencies of the swimmers is shown in Figs. 14(b) and 14(d) for the sheets and the filaments, respectively. Compared to that of a single swimmer, the efficiency is greatly enhanced when the asymmetric swimmers attract for both the sheets and the filaments. However, the pair of filaments in 3D enjoys a sixty percent increase in efficiency compared to only a forty five percent increase for the sheets.

In the previous example, when the flagella were initialized at a distance of $d = 0.4$ apart, the trajectories and process of attraction are similar for the sheets and filaments (Figs. 12 and 13). In contrast, we have found qualitatively different dynamics between the interacting sheets and the interacting filaments for a range of initial distances between the asymmetric swimmers. If far enough apart, the interacting swimmers will pursue the circular trajectories of a solo swimmer. If close enough together, the flagella attract in spite of their asymmetric waveform. Here, we choose the initial distance in an intermediate range and compare the behavior of sheets and filaments. The flow fields and flagellar waveforms for sheets initialized at $d = 0.5$ apart in a 2D fluid are shown in Fig. 15. We see that the swimmers are not able to fully attract before entering their circular trajectories, shown in Fig. 16(a). After the 2D asymmetric swimmers push away from each other, they each swim in a circular trajectory similar to the solo asymmetric swimmer in Fig. 11(a). Fig. 16(b) shows the temporal evolution of the normalized efficiency of each of these interacting sheets. Since each asymmetric swimmer settles into a circular trajectory close to that of a solo swimmer, the normalized efficiencies go to one.

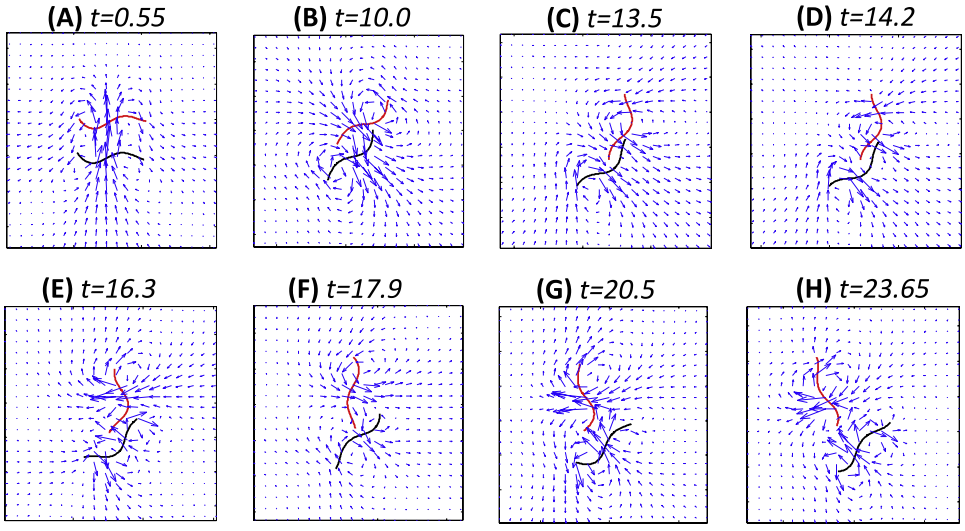


FIG. 15. The 2D flow field is shown at various time points for the asymmetric sheets. In this simulation, the sperm are initialized $d = 0.5$ apart. The corresponding trajectories are shown in Fig. 16(a).

For the same initial distance of $d = 0.5$ apart, we see very different behaviors for the 3D filaments. Fig. 17 shows that the asymmetrically driven filaments begin pursuing circular trajectories, but settle into an in-tandem state as the head point of the flagellum initially at the bottom aligns with the tail point of the flagellum initially at the top. In the 2D case shown in Fig. 15, the flow field pushed the swimmers away from each other. In the case of the 3D swimmers shown in Fig. 17, we observe that the filaments are able to maintain alignment for over 60 flagellar beat periods.

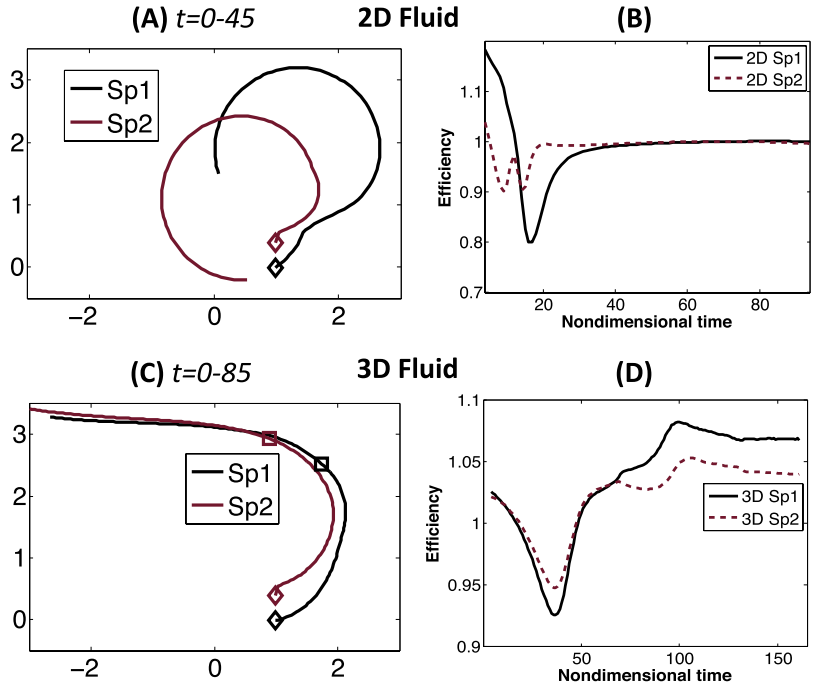


FIG. 16. (a) Trajectories of head points of sheets in a 2D fluid corresponding to Fig. 15. (b) Temporal evolution of the efficiencies of the sheets normalized by the efficiency of the corresponding solo swimmer. (c) Trajectories of head points of filaments in a 3D fluid corresponding to Fig. 17. (d) Temporal evolution of the efficiencies of the filaments normalized by the efficiency of the corresponding solo swimmer. Diamonds denote starting points, and rectangles denote the time at which repulsion is first turned on.

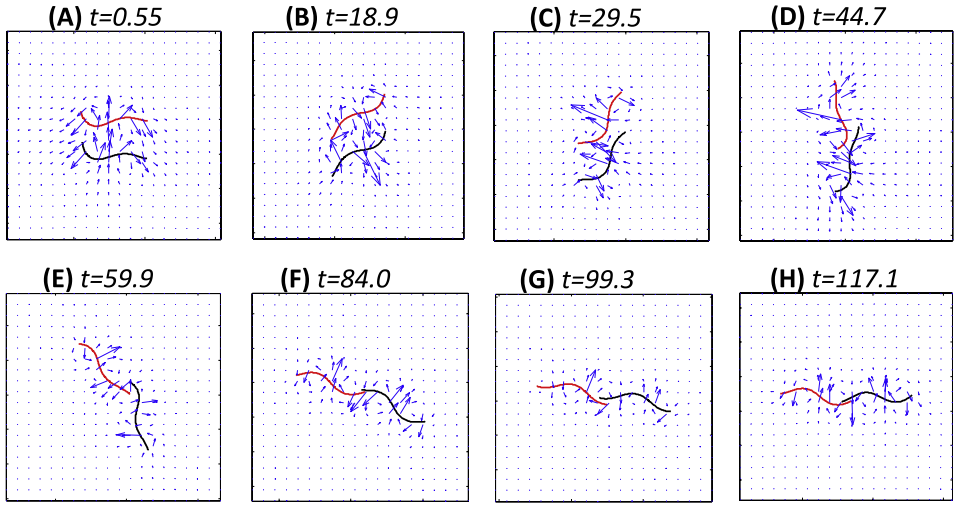


FIG. 17. The 3D flow field in the plane of the swimmer is shown at various time points for the asymmetric filaments. In this simulation, the sperm are initialized $d = 0.5$ apart. This corresponds to the trajectory in Fig. 16(c).

The corresponding trajectories of the head points of the 3D filaments initialized $d = 0.5$ apart are shown in Fig. 16(c). We can see that the sperm start out on circular trajectories, align, and then maintain an approximately straight path. This path curvature is $c_{3D} = 0.06$, while that of the solo swimmer is $c_{3D} = 0.75$. The temporal evolution of the normalized efficiencies for the aligned swimmers are shown in Fig. 16(d). As the asymmetric swimmers begin to align, the normalized efficiency decreases. When the swimmers are able to align around $t = 70$, the efficiency of each filament is greater than that of a single asymmetric swimmer. The swimming speed of the aligned asymmetric swimmers is approximately the same as that of the corresponding solo swimmer.

The alignment of two coplanar swimmers propagating asymmetric beatforms in Figs. 16(c) and 17 is stable; the alignment occurs for more than 60 flagellar beats. In Figs. 18(a) and 18(b), we summarize the results for sheets and filaments for five different initialized vertical distances and three bending moduli. The alignment symbol is used when this behavior lasts for more than 30 beat periods of the simulation. We examine data from simulations for 100 beat periods that should be representative of the long-time interaction. For 2D sheets in Fig. 18(a), we observe very different behaviors based on the stiffness. The stiffest sheets repulse at all of the initial vertical distances (repulsion could be after a few beat periods or after several beat periods when and circular trajectories are initiated). At the initial distance of 0.5 and 0.6, the asymmetric 2D sheets with small bending stiffness are able to

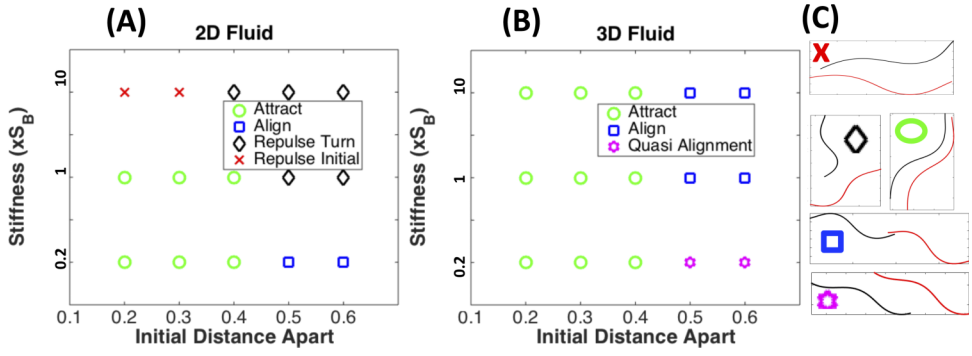


FIG. 18. Interactions of asymmetric swimmers for different initialized vertical distance apart and bending stiffness $S_B$. (a) 2D sheets exhibit attraction, alignment, and repulsion. (b) Asymmetric filaments exhibit attraction, alignment (>30 beats), and quasi-alignment (<50) beats. All symbols denote the behavior of the system up to 100 beat periods. (c) Representative snapshots of flagellar arrangement in a simulation corresponding to symbols in panels (a) and (b).

align. However, the moderate and large bending stiffnesses prevent these swimmers from aligning and they end up moving apart. The asymmetric 3D filaments exhibit similar behaviors as the bending stiffness is varied for initial vertical distances of less than 0.4. For the case of 0.5 and 0.6, we observe that the asymmetric floppier filament aligns on a much slower time scale than in the stiffer cases. We call this quasi alignment in Fig. 18(b) and a representative configuration is shown in panel 18(c); the two swimmers are attracting but have not reached a state with a small region of close overlap as in the aligned case, also depicted in panel 18(c).

## IV. DISCUSSION

In this study, we have examined the synchronization and attraction of coplanar, flexible, finite length sheets and filaments with preferred kinematics. The most important feature of these investigations is the elastohydrodynamic coupling whereby the kinematics of the sheets and filaments change depending upon both the fluid dynamics and their interactions. We observed that two symmetric swimmers will synchronize within a few beats, with time to synchronization depending upon on their initial distance apart, phase difference, and bending stiffnesses. This fast time scale of synchronization has been reported in other computational studies.[10–12] We observed that in general, synchronization was stronger in 2D. Our simulation results agree with the previous theoretical results that assert that the in-phase configuration of infinite sheets and filaments is most energetically favorable.[1–3,8] For the first time, we have shown that 3D filaments exhibit a time to phase locking that depends non-monotonically on the bending stiffness. Additionally, the 2D sheets generally exhibit a decreased synchronization time as bending stiffness is increased.

Attraction occurs on a longer time scale. In 3D, we show that sufficiently stiff finite length filaments increase their efficiencies when attracted. These results are similar to the 2D results of Yang *et al.*,[12] where a model using multiparticle collision dynamics showed a decrease in energy consumption as the distance between sperm decreased. Our 3D computational results also show an enhancement in swimming speed for symmetric, attracted filaments. This is similar to experimental results where attracted and synchronized bull sperm had an increased swimming speed in comparison to a single sperm.[4] For the 2D swimmers, the time to attraction was independent of the initial separation distance (for $d = 0.25$, 0.5, and 0.75), whereas the time to attraction increased as separation distance increased for the 3D filaments. It is well known that hydrodynamic interactions of two pushers will result in attraction[34] and a finite length flagellar swimmer (with no cell body) can be considered a weak pusher. In the future, it will be interesting to explore reduced models of swimmers in an effort to completely characterize the attraction behavior as a function of elasticity. In this study, we offer more detailed simulations as a touchstone for such reduced models. Future models will also investigate how the dynamics or attraction vary with different horizontal placements of the swimmers.

We also examined the interaction of sheets and filaments whose preferred waveforms were asymmetric, similar to hyperactivated motility patterns of mammalian sperm.[14,35] In the case of 3D filaments, we found that two coplanar swimmers could settle into a steady aligned state where the filaments progressed in tandem. This alignment is robust for 3D planar filaments and only occurs for floppy 2D sheets. This two-sperm "train" is reminiscent of those found in populations of wood mice, whose sperm form "trains" of about 1 mm in length that swim in an approximately linear trajectory.[36] In these configurations, mechanical attachment of neighboring sperm was observed between the apical hook of the head of one sperm to the flagellum or apical hook of another. In other experiments with bull sperm, it has been observed that synchronized and attracted sperm swimming transversely have a rigid attachment between their heads.[4]

Motivated by understanding the differences between 2D and 3D hydrodynamics of actuated elastic flagella, we considered the idealized case where no out of plane perturbations of the coplanar filaments occurred. However, recent models that do consider such perturbations demonstrate that a coplanar arrangement of filaments is an unstable configuration.[37,38] This suggests that while hydrodynamic interactions may initiate the formation of sperm trains, mechanical attachments are necessary for their persistence.

The composition of the fluid that a sperm will swim in can vary greatly. In this study, we focused on a purely Newtonian fluid in the Stokes regime. Experiments have shown that flagellar waveforms vary with fluid properties.[21,39] In the mammalian reproductive tract, fluid can contain cellular debris, proteins, hormones, and ions.[40,41] The protein structure and organization can greatly change the fluid properties; cervical mucus, due to large amounts of the protein mucin, can be considered a viscoelastic fluid.[42] Recent computational studies have explored the effects of viscoelasticity on idealized swimmers of infinite and finite lengths using an Oldroyd-B model in a 2D fluid.[9,16,43] Finite elastic filaments whose preferred kinematics reflected an increasing amplitude along their length were found to achieve enhanced swimming speeds when the frequency of the tail beat was matched with polymer relaxation times.[16] A recent study has characterized bending rigidities and preferred kinematics that allow for such elastic enhancement in finite length swimmers.[43] While phase-locking of two actuated, infinite elastic sheets has been demonstrated in a 2D Oldroyd-B fluid,[9] phase-locking or attraction of finite sheets in 2D has not. In addition, the interaction of coplanar filaments in a 3D viscoelastic fluid has not yet been described. It will be very interesting to extend the present study of interacting sheets and filaments to the one that incorporates fluid viscoelasticity.

## ACKNOWLEDGMENTS

The work of S. Olson was supported, in part, by NSF DMS 1122461. The work of L. Fauci was supported, in part, by NSF DMS 1043626 and NSF DBI 1062052.

[1] G. Taylor, "Analysis of the swimming of microscopic organisms," Proc. R. Soc. London, Ser. A **209**, 447–461 (1951).
[2] G. Taylor, "The action of waving cylindrical tails in propelling microscopic organisms," Proc. R. Soc. London, Ser. A **211**, 225–239 (1952).
[3] C. Mettot and E. Lauga, "Energetics of synchronized states in three-dimensional beating flagella," Phys. Rev. E **84**, 061905-1–061905-14 (2011).
[4] D. Woolley, R. Crockett, W. Groom, and S. Revell, "A study of synchronisation between the flagella of bull spermatozoa, with related observations," J. Exp. Biol. **212**, 2215–2223 (2009).
[5] G. Elfring and E. Lauga, "Hydrodynamic phase locking of swimming microorganisms," Phys. Rev. Lett. **103**, 088101 (2009).
[6] G. Elfring and E. Lauga, "Passive hydrodynamic synchronization of two-dimensional swimming cells," Phys. Fluids **23**, 011902 (2011).
[7] G. Elfring, O. Pak, and E. Lauga, "Two-dimensional flagellar synchronization in viscoelastic fluids," J. Fluid Mech. **646**, 505–515 (2010).
[8] G. Elfring and E. Lauga, "Synchronization of flexible sheets," J. Fluid Mech. **674**, 163–173 (2011).
[9] J. Chrispell, L. Fauci, and M. Shelley, "An actuated elastic sheet interacting with passive and active structures in a viscoelastic fluid," Phys. Fluids **25**, 013103-1–013103-16 (2013).
[10] L. Fauci, "Interaction of oscillating filaments: A computational study," J. Comput. Phys. **86**, 294–313 (1990).
[11] L. Fauci and A. McDonald, "Sperm motility in the presence of boundaries," Bull. Math. Biol. **57**, 679–699 (1995).
[12] Y. Yang, J. Elgeti, and G. Gompper, "Cooperation of sperm in two dimensions: Synchronization, attraction, and aggregation through hydrodynamic interactions," Phys. Rev. E **78**, 061903-1–061903-9 (2008).
[13] H. Ho and S. Suarez, "Hyperactivation of mammalian spermatozoa: Function and regulation," Reproduction **122**, 519–526 (2001).
[14] S. Suarez, "Control of hyperactivation in sperm," Hum. Reprod. Update **14**, 647–658 (2008).
[15] L. Fauci and C. Peskin, "A computational model of aquatic animal locomotion," J. Comput. Phys. **77**, 85–108 (1988).
[16] J. Teran, L. Fauci, and M. Shelley, "Viscoelastic fluid response can increase the speed of a free swimmer," Phys. Rev. Lett. **104**, 038101-1–038101-4 (2010).
[17] S. Olson, S. Suarez, and L. Fauci, "Coupling biochemistry and hydrodynamics captures hyperactivated sperm motility in a simple flagellar model," J. Theor. Biol. **283**, 203–216 (2011).
[18] J. Simons, S. Olson, R. Cortez, and L. Fauci, "The dynamics of sperm detachment from epithelium in a coupled fluid-biomechanical model of hyper activated motility," J. Theor. Biol. **354**, 81–94 (2014).
[19] R. Cortez, "The method of regularized Stokeslets," SIAM J. Sci. Comput. **23**, 1204–1225 (2001).
[20] R. Cortez, L. Fauci, and A. Medovikov, "The method of regularized Stokeslets in three dimensions: Analysis, validation, and application to helical swimming," Phys. Fluids **17**, 031504-1–031504-14 (2005).
[21] D. Smith, E. Gaffney, H. Gadelha, N. Kapur, and J. Kirkman-Brown, "Bend propagation in the flagella of migrating human sperm, and its modulation by viscosity," Cell Motil. Cytoskeleton **66**, 220–236 (2009).
[22] L. Burkman, "Discrimination between nonhyperactivated and classical hyperactivated motility patterns in human spermatozoa using computerized analysis," Fertil. Steril. **55**, 363–371 (1991).
[23] B. Marquez, G. Ignotz, and S. Suarez, "Contributions of extracellular and intracellular $Ca^{2+}$ regulation of sperm motility: Release of intracellular stores can hyperactivate CatSper1 and CatSper2 null sperm," Dev. Biol. **303**, S1214–S1221 (2007).
[24] R. DeMott and S. Suarez, "Hyperactivated sperm progress in the mouse oviduct," Biol. Reprod. **46**, 779–785 (1992).
[25] D. Woolley and G. Vernon, "Functional state of the axonemal dyneins during flagellar bend propagation," Biophys. J. **83**, 2162–2169 (2002).

[26] G. Vernon and D. Woolley, "Basal sliding and the mechanics of oscillation in a mammalian sperm flagellum," Biophys. J. **87**, 3934–3944 (2004).
[27] D. Woolley, "Flagellar oscillation: A commentary on proposed mechanisms," Biol. Rev. **85**, 453–470 (2010).
[28] L. Fauci and R. Dillon, "Biofluidmechanics of reproduction," Annu. Rev. Fluid Mech. **38**, 371–394 (2006).
[29] S. Olson, "Fluid dynamic model of invertebrate sperm motility with varying calcium inputs," J. Biomech. **46**, 329–337 (2013).
[30] J. Cummins and P. Woodall, "On mammalian sperm dimensions," J. Reprod. Fertil. **75**, 153–175 (1985).
[31] K. Schmitz-Lesich and C. Lindemann, "Direct measurement of the passive stiffness of rat sperm and implications to the mechanism of the calcium response," Cell Motil. Cytoskeleton **59**, 169–179 (2004).
[32] K. Lesich, D. Pelle, and C. Lindemann, "Insights into the mechanism of ADP action of flagellar motility derived from studies of bull sperm," Biophys. J. **95**, 472–482 (2008).
[33] Y. Yang, V. Marceau, and G. Gompper, "Swarm behavior of self-propelled rods and swimming flagella," Phys. Rev. E **82**, 031904-1–031904-13 (2010).
[34] E. Lauga and T. Powers, "The hydrodynamics of swimming microorganisms," Rep. Prog. Phys. **72**, 096601 (2009).
[35] S. Suarez and A. Pacey, "Sperm transport in the female reproductive tract," Hum. Reprod. Update **12**, 23–37 (2006).
[36] H. Moore, K. Dvorakova, N. Jenkins, and W. Breed, "Exceptional sperm cooperation in the wood mouse," Nature **418**, 174–177 (2002).
[37] I. Llopis, I. Pagonabarraga, M. C. Lagomarsino, and C. Lowe, "Cooperative motion of intrinsic and actuated semiflexible swimmers," Phys. Rev. E **87**, 032720 (2013).
[38] J. Simons, L. Fauci, and R. Cortez, "A fully three-dimensional model of the interaction of driven elastic filaments in a Stokes fluid with applications to sperm motility," J. Biomech. Eng. **48**, 1639–1651 (2015).
[39] D. Woolley and G. Vernon, "A study of helical and planar waves on sea urchin sperm flagella, with a theory of how they are generated," J. Exp. Biol. **204**, 1333–1345 (2001), available at http://jeb.biologists.org/content/jexbio/204/7/1333.full.pdf.
[40] S. Lai, Y. Wang, D. Wirtz, and J. Hanes, "Micro- and macrorheology of mucus," Adv. Drug Delivery Rev. **61**, 86–100 (2009).
[41] A. Wiede, M. Hinz, E. Canzler, K. Franke, C. Quednow, and W. Hoffman, "Synthesis and localization of the mucin-associated TFF-peptides in the human uterus," Cell Tissue Res. **303**, 109–115 (2001).
[42] J. Rutllant, M. Lopez-Bejar, P. Santolaria, J. Yaniz, and F. Lopez-Gatius, "Rheological and ultrastructural properties of vaginal fluid obtained at oestrus," J. Anat. **201**, 53–60 (2002).
[43] B. Thomases and R. D. Guy, "Mechanisms of elastic enhancement and hindrance for finite-length undulatory swimmers in viscoelastic fluids," Phys. Rev. Lett. **113**, 098102 (2014).